



Detailed Morphologic Mapping and Traverse Planning for a Rover-based Lunar Sample Return Mission to Schrödinger Basin

Zachary R. Morse^{1,2} , Gordon R. Osinski^{3,4}, Livio L. Tornabene^{3,4}, Matthew Bourassa⁵, Michael Zanetti⁶, Patrick J. A. Hill⁷, Eric Pilles^{3,4}, Matthew Cross^{3,5}, Derek King^{3,4}, and Gavin Tolometti^{3,4}

¹ Department of Physics and Astronomy, Howard University, 2400 Sixth Street NW, Washington, DC 20059, USA

² NASA Goddard Space Flight Center, 8800 Greenbelt Road, Greenbelt, MD 20771, USA

³ Institute for Earth and Space Exploration, University of Western Ontario, 1151 Richmond Street, London, ON N6A 5B7, Canada

⁴ Department of Earth Sciences, University of Western Ontario, 1151 Richmond Street, London, ON N6A 5B7, Canada

⁵ Department of Electrical and Computer Engineering, University of Western Ontario, 1151 Richmond Street, London, ON N6A 5B7, Canada

⁶ Marshall Space Flight Center, Huntsville, AL 35805, USA

⁷ Department of Earth and Atmosphere, University of Alberta, Edmonton, AB, Canada

Received 2020 October 30; revised 2021 May 27; accepted 2021 May 31; published 2021 August 17

Abstract

Schrödinger basin, a 312 km diameter complex impact structure located near the lunar south pole, has been widely cited as a prime target for future lunar exploration. In 2020 NASA identified Schrödinger as a high-priority landing site for a 2024 mission supported by the Payloads and Research Investigations on the Surface of the Moon solicitation and the Commercial Lunar Payload Services program. Schrödinger basin hosts an uplifted peak ring that would provide a surface mission with access to materials that originated deep within the lunar crust, as well as material ejected from the larger South Pole–Aitken basin. Schrödinger basin also hosts well-preserved mare and pyroclastic deposits that could provide valuable insight into volcanic processes on the Moon. This study used high-resolution Wide Angle Camera and Narrow Angle Camera images from the Lunar Reconnaissance Orbiter, elevation data from the Lunar Orbiter Laser Altimeter, and spectral data from the Clementine mission to produce a high-resolution morphologic map of the basin center consisting of 10 distinct morphologic units. This new map was used to plan traverse paths for a rover mission to the region. The design requirements for this traverse were based on those originally developed for the multiagency Human-Enhanced Robotic Architecture and Capability for Lunar Exploration and Science (HERACLES) mission and the Canadian Space Agency Precursor to Humans And Science Rover concept. The proposed traverse path includes up to 20 sample collection stops with the goal of better understanding lunar chronology, lunar volcanism, and the impact cratering process.

Unified Astronomy Thesaurus concepts: [Lunar impacts \(958\)](#); [Lunar surface \(974\)](#); [Rovers \(1409\)](#); [Lunar craters \(949\)](#); [Lunar composition \(948\)](#); [Lunar science \(972\)](#)

1. Introduction

Schrödinger basin is a 312 km diameter impact structure centered at (75.0° S 132.4° E), located on the lunar farside and near the south pole of the Moon (Figure 1). Schrödinger is considered one of the best-preserved examples of a peak ring impact basin in the solar system (e.g., Wilhelms et al. 1979; Shoemaker et al. 1994), yet to date it has not been visited by a lunar surface exploration mission. Beyond the well-preserved peak ring structure, Schrödinger hosts a number of additional intriguing geologic features, including a network of extensional grabens, multiple volcanic deposits, ejecta material from several external subsequent impact events, and potentially material uplifted from the massive South Pole–Aitken basin (SPA). All of these features have made Schrödinger a likely target for near-future surface missions and the subject of numerous studies in preparation for the Artemis generation of lunar exploration (e.g., Kring et al. 2014, 2016; Steenstra et al. 2016). In this study, we contribute to this growing body of work by conducting the most detailed morphologic mapping of the central basin region produced to date. This new mapping and analysis of basin materials were used as the basis to

produce a proposed rover traverse, including a list of potential stops featuring geologically significant and easily accessible targets, for a future rover-based sample return mission to the inner Schrödinger region. The results of this work are also equally applicable for future human missions to this site.

2. Background

2.1. Geologic Setting

Schrödinger basin measures ~312 km in diameter and has an average depth of 4.5 km. The basin features a peak ring structure that is ~150 km in diameter and rises up to ~3 km above the primarily flat-lying impact and volcanic deposits covering the basin floor. The age for Schrödinger is estimated to be ~3.8 Ga (Wilhelms et al. 1979; Shoemaker et al. 1994; Kramer et al. 2013; Kring et al. 2016), and the basin structure is considered to be one of the best-preserved examples of a peak ring basin on the lunar surface (Shoemaker et al. 1994; Kring et al. 2016). The basin floor also hosts volcanic features, including both mare and pyroclastic deposits, as well as a network of extensional grabens (Figure 1; Wilhelms et al. 1979; Shoemaker et al. 1994; Gaddis et al. 2003; Mest 2011; Kramer et al. 2013; Shankar et al. 2013). Schrödinger basin is situated inside the southern rim of SPA, the largest and oldest impact structure observed on the lunar surface (Figure 1; Wilhelms et al. 1979). In a 2007 report, the National Research



Original content from this work may be used under the terms of the [Creative Commons Attribution 4.0 licence](#). Any further distribution of this work must maintain attribution to the author(s) and the title of the work, journal citation and DOI.

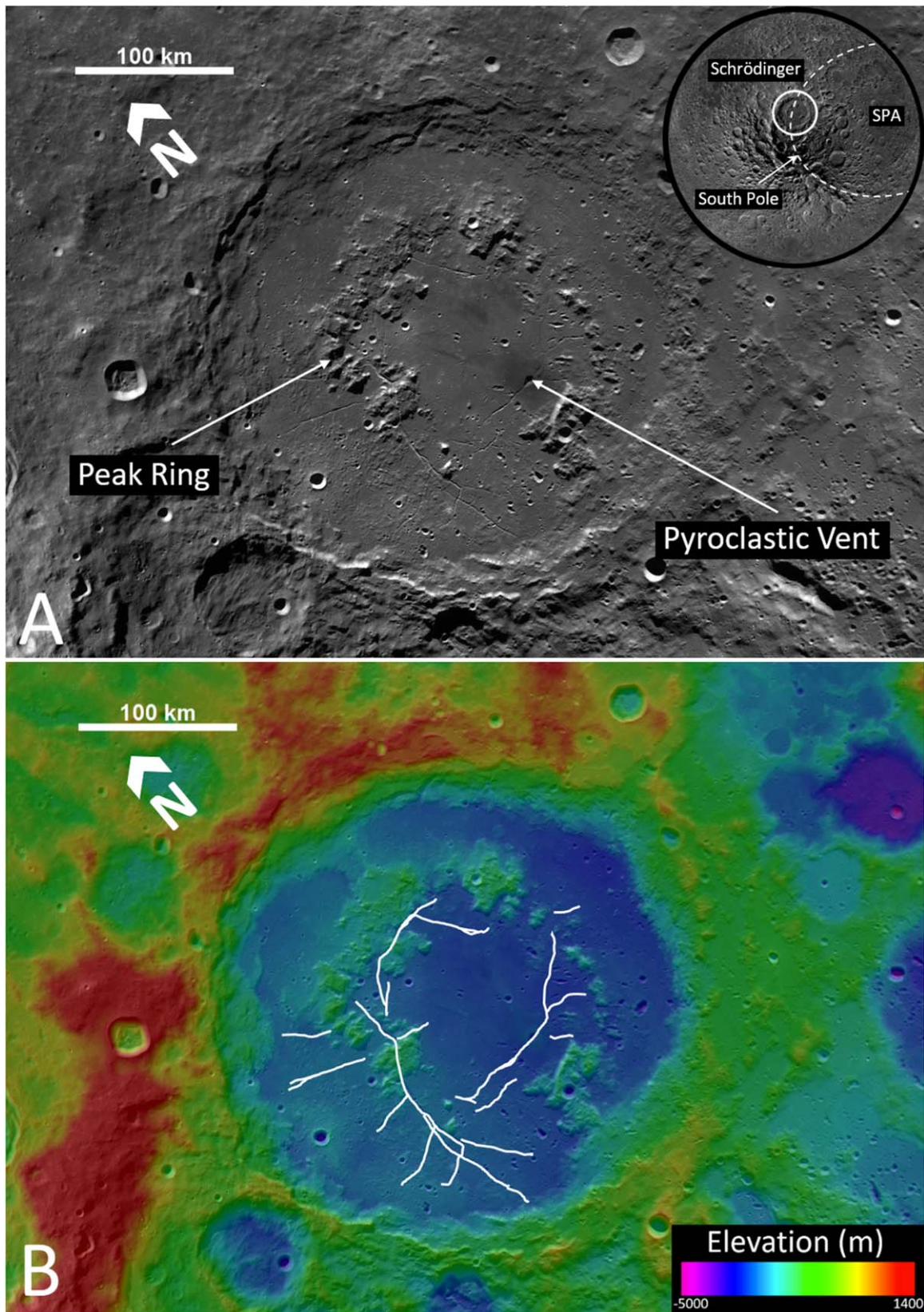


Figure 1. (A) Schrödinger basin in LROC-WAC mosaic. The inset image shows the position of Schrödinger basin relative to the lunar south pole and the outline of SPA. (B) Same perspective overlaid with LOLA 1024 PPD elevation data, colorized as indicated in the inset key to illustrate topographic changes within and around Schrödinger basin. White lines indicate the extent of the series of grabens running throughout the basin floor. Base Image Credit: NASA/GSFC/ASU.

Council (NRC) identified several high-priority science goals related to SPA, including (1a) test the cataclysm hypothesis by determining the spacing in time of the creation of lunar basins

and (1b) anchor the early Earth–Moon impact flux curve by determining the age of the oldest lunar basin (SPA; National Research Council 2007). Dating material from the SPA impact

would greatly enhance our understanding of lunar surface chronology and provide insight into the timing and extent of the Late Heavy Bombardment of the inner solar system (Hurwitz & Kring 2015). Due to the uplift associated with impact crater central peak and peak ring formation, it has been proposed that the Schrödinger peak ring structure is partially composed of SPA material excavated from depth (Kramer et al. 2013; Kring et al. 2016). This makes Schrödinger basin an ideal target for a sample return mission given the potential of sampling impact materials of a wide range of ages. Analysis of samples from this region would provide the opportunity to perform dating analysis that would place constrained ages on both the Schrödinger and SPA impact structures. The presence of the aforementioned volcanic materials also makes Schrödinger a target of significant interest owing to the potential presence of trace amounts of volatiles within the volcanic materials that would indicate potential for future in situ resource utilization processes (Kring et al. 2014; Steenstra et al. 2016; Needham & Kring 2017; Head et al. 2020), in addition to answering fundamental questions about lunar volcanism, particularly on the lunar farside.

2.2. Motivation for Study

In July of 2020, NASA announced that the Payloads and Research Investigations on the Surface of the Moon (PRISM) solicitation would include Schrödinger basin as a target for a lunar surface mission in late 2024. The scientific payload for this proposed mission is set to be delivered to the lunar surface aboard a lander provided as part of the Commercial Lunar Payload Services (CLPS) program and may include static lander mounted instrumentation, as well as a rover. The goal of this work was to investigate the potential scientific return of a robotic sample return mission to the interior of Schrödinger basin and design a traverse plan and concept of operations for such a mission. While this work was based on the early framework of the Human-Enhanced Robotic Architecture and Capability for Lunar Exploration and Science (HERACLES) mission concept—an ongoing collaboration between the Canadian Space Agency (CSA), European Space Agency, and Japan Aerospace Exploration Agency (JAXA)—it is applicable to other missions and scenarios. The primary goal of the original HERACLES mission concept was to use a human-assisted rover platform to collect geologic samples of lunar surface material for return to Earth (Landgraf 2016; Hiesinger et al. 2019). Current plans related to the HERACLES mission concept have evolved away from the inclusion of a lunar surface rover, but the study detailed here still provides valuable information for other future lunar surface missions considering Schrödinger basin as a landing site, including the proposed NASA PRISM/CLPS mission. As part of the initial HERACLES effort, the CSA conducted a Science Maturation Study to investigate the design and implementation of their Precursor to Humans And Science Rover (PHASR) concept (Osinski et al. 2019). This contribution is a product of this CSA-funded PHASR study.

2.3. Mission Design Requirements

The HERACLES mission architecture on which this work was based had proposed sending a lander with a rover platform to the lunar surface. A precision landing ellipse of 100 m was given as part of the original mission concept. Both the lander and

rover hardware would be designed to survive through a minimum of two lunar night cycles. This would enable a total primary mission time of approximately 1130 hr of operation, or 47 Earth-days. Assuming a maximum traverse speed of 2 kph similar to that of the Soviet Lunokhod Rovers (Ellery 2016), this proposed length of mission could allow for an absolute maximum rover traverse distance of approximately 85 km across the lunar surface, including up to 20 stops for analysis and sampling of lunar material. Allowing an ample margin for both error and safety, we developed a traverse plan in the range of 40–50 km (see Section 6). The rover proposed as part of the original HERACLES mission concept was envisioned to include a sample container capable of holding up to 16 kg of lunar surface material. While the exact design of a future sample container was not specified as part of this maturation study, the included traverse was designed around the idea that the sample storage mechanism would comprise multiple separate collection tubes that would be independently sealed after sampling, similar to the Sample Caching System used on the Mars 2020 mission (Boeder & Soares 2020). In this mission concept, the sample container must be returned to the lander in order to return the collected samples to Earth for additional laboratory analysis. Thus, any proposed traverse plan must be a closed loop, starting and ending at the lander platform. An orbital asset for communications relay such as the Lunar Gateway was also included as part of the original mission concept, so direct line of site to Earth was not considered a limitation for planning the proposed rover traverse.

2.4. PHASR Science Goals

The CSA PHASR maturation study identified four main areas of scientific investigation that guided the selection of a landing region and the potential sample locations where materials would be collected (Osinski et al. 2019). Four priority science themes were defined:

1. *Impact Cratering Processes:* Acquire samples and in situ measurements of Schrödinger basin impactites to provide insight into peak ring basin formation, impact melting, and shock metamorphic processes and to understand the provenance of uplifted and excavated lunar crustal materials.

2. *Lunar Chronology:* Return lunar samples to Earth from Schrödinger basin in order to constrain the early bombardment history of the solar system, characterize the lunar crust, and constrain the thermal evolution of the Moon.

3. *Lunar Volcanism:* Acquire samples and in situ measurements of mare and pyroclastic volcanic deposits within Schrödinger basin to provide a clear view of the overall history of lunar volcanism and its relation to the Moon's thermal and compositional evolution.

4. *Prepare for the Return of Humans to the Lunar Surface:* Analyze the topographic, radiation, and temperature environments on the lunar surface and search for trace evidence of volatiles within Schrödinger basin in order to provide important information for future human activity on the Moon.

2.5. Previous Mapping Efforts

As Schrödinger basin has been a target of great interest for future lunar surface missions, geologic maps of the basin as a whole have been continually updated as modern remote sensing data sets become more detailed. Previous mapping efforts include Shoemaker et al. (1994), Mest (2011), Kramer et al. (2013), and

Shankar et al. (2013). Each of these maps identifies key features of the basin interior, including the peak ring, mare units, and pyroclastic deposits. Each of these previous works also identifies and maps the distinct network of extensional grabens running throughout the basin interior. However, there are several subtle differences between the previously completed maps in terms of exact shape and extent of individual unit borders and in how the basin floor is divided into subunits of geologic materials. For example, Shoemaker et al. (1994) divided the basin floor into four facies based on surface texture, morphology, and albedo using data from the Clementine mission, while Mest (2011) mapped the basin floor as composed of five morphologically distinct units based on surface texture, albedo, superposition, and cross-cutting relationships with surrounding units using data obtained by the Lunar Reconnaissance Orbiter (LRO). Kramer et al. (2013) divided the basin floor into six morphologically and compositionally distinct units based on surface texture and spectral data from the Moon Mineralogy Mapper (M^3). Shankar et al. (2013) instead present the basin floor as a single unit identified as interior impact melt material. Following the site selection workshop described below (Section 3), we focused our analysis in the region interior to the peak ring. While this region has been mapped previously, we felt that a more detailed map focusing on our specific region of interest (see Section 3.1) was important for identifying small morphologically distinct features, traversable regions, and targets for potential sample acquisition based on the PHASR science goals. In contrast with previous works, our new map divides the basin floor into two separate morphologic units: smooth and hummocky. As discussed later, this subdivision of the basin floor has implications not only for the nature of the crater-fill impactites at Schrödinger (e.g., clast-rich vs. clast-poor impact melt rocks) but also for rover navigation. Our new map also displays much greater detail around our chosen landing site than any of the previous maps of the region, including the identification of individual boulders ≥ 5 m in scale (see Section 4.1 for additional details).

Due to the abundance of high-priority scientific targets and diverse geology found within Schrödinger, several previous studies have also proposed traverse paths and potential sampling sites within the basin, including O’Sullivan et al. (2011), Kramer et al. (2013), Potts et al. (2015), Steenstra et al. (2016), and Allender et al. (2019). While these studies do also identify similar sites of interest (SOIs) within the Schrödinger volcanic deposits and peak ring, the traverse paths and potential sampling locations presented in this science maturation study were derived independently and are based wholly on available remote sensing data sets analyzed through the PHASR site selection workshop described below in Section 3.

3. Methods

3.1. Identification of Sites of Interest

A landing site selection workshop was held at Western University in order to identify the best study area within Schrödinger basin. Such an area would host a large number of SOIs within close proximity to one another, which when visited *in situ* could provide the greatest amount of scientific information related to the established PHASR science goals (Section 2.4). During the site selection workshop, researchers studied high-resolution remote sensing data sets, including 100 m pixel^{-1} LROC-WAC and 0.5 m per pixel LROC-NAC

images along with 1024 PPD Lunar Orbiter Laser Altimeter (LOLA) topographic elevation data and Clementine compositional data sets covering the interior of Schrödinger basin. The group identified any SOIs of morphologic or compositional importance within the interior of the basin and sorted all identified SOIs into one of the following categories: mare material, pyroclastic material, floor material, peak ring material, post-Schrödinger impact crater material, floor graben, or “other.” Preference was given to locations where a sample could be obtained either via a drill core into solid rock such as a large boulder or via a scoop sample of unconsolidated material such as regolith. A total of 186 locations of significant scientific interest were identified, and a representative point for each location was mapped within Schrödinger. The resulting geographic distribution of points helped the team identify which region within Schrödinger contained the greatest density of features of high scientific value (Figure 2). Following an open discussion among workshop participants, a region in the northern half of the basin center, within the interior of the peak ring, was chosen as the target region for the proposed rover traverse, as it hosted the densest population of high-priority science target locations (Figure 2). A short and efficient nominal traverse within this proposed region would enable the rover to visit a number of geologically diverse sites and collect a representative suite of samples that address questions associated with all four of the main science themes established as part of the PHASR maturation study. Visiting this selected region would also allow the rover to access other, more distant parts of the basin interior during any potential extended mission beyond the main sample collection and return period.

3.2. Remote Sensing Analysis

Following the workshop, a mapping effort was focused on the northern interior part of the peak ring and basin center identified as the area with the greatest number of SOIs. This analysis and mapping of the Schrödinger basin floor relied on several high-resolution data sets obtained by NASA’s LRO. These include $\sim 100\text{ m pixel}^{-1}$ images taken by the Lunar Reconnaissance Orbiter Wide Angle Camera (LROC-WAC; Robinson et al. 2010), $\sim 0.5\text{ m pixel}^{-1}$ images taken by the Lunar Reconnaissance Orbiter Camera—Narrow Angle Camera (LROC-NAC), $10\text{--}50\text{ cm}$ vertical resolution elevation data derived from the Lunar Orbiter Laser Altimeter (LOLA) on board LRO (Chin et al. 2007), and circular polarization ratio (CPR) data derived from the Miniature Radio Frequency (Mini-RF) instrument on board LRO. Additionally, we used FeO abundance maps created using Clementine spectral data (Lucey et al. 1995; Blewett et al. 1997) to differentiate between the relatively iron-rich volcanic deposits and the relatively iron-poor surrounding basin materials. The combination of all of these data products enabled us to analyze the surface morphology of the basin floor and surrounding peak ring in order to subdivide the region into distinct units based on observed surface texture, relative tonality, the expression of topographic structures, and relationship with preexisting topography.

Certain areas, including the immediate region surrounding the proposed landing site, were observed and mapped in greater detail using the $\sim 0.5\text{--}1\text{ m pixel}^{-1}$ LROC-NAC images. The use of the high-resolution NAC images allowed for the identification of small spatial scale features ($>3\text{ m}$ in size).

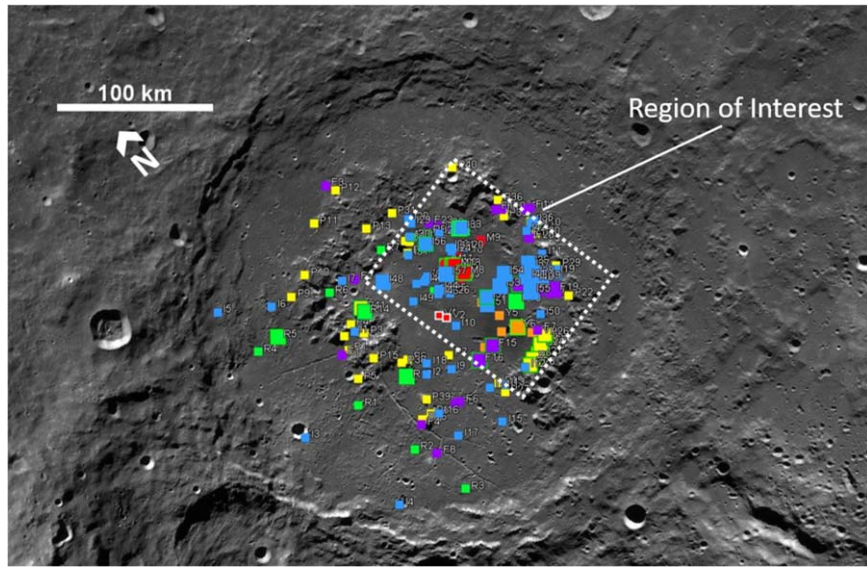


Figure 2. LROC-WAC image of Schrödinger basin. Points of significant scientific interest as identified during the landing site selection workshop are illustrated within the basin and colorized based on broad categories as follows: red—mare deposits; orange—pyroclastic deposits; yellow—peak ring material; green—post-Schrödinger impact materials; blue—extensional graben material; purple—basin floor materials. The white dashed box represents the region of greatest point density that was selected for further study. Base Image Credit: NASA/GSFC/ASU.

The high-resolution images were also used to refine boundaries between different morphologic units and provide fine-scale context for different remote sensing data sets (listed above). This level of detail near the landing site allowed us to identify potential obstacles to both landing and initial rover traverses, as well as select potential sampling locations near the landing site where the initial samples could be obtained.

We used the Java Mission-planning and Analysis for Remote Sensing (JMARS) program (Christensen et al. 2009) to map unique geomorphologic units of Schrödinger impact materials and post-impact deposits in the basin interior by drawing polygons to encompass the extent of regions displaying like-geomorphologic characteristics. We also used JMARS to document the measured surface area, geographic setting, and stratigraphic relationship of each mapped unit as discussed in the following sections.

3.3. Traverse Planning

Utilizing the points of interest generated during the landing site workshop and the unit interpretations of the new morphologic mapping detailed below, we created an example rover traverse plan designed to explore portions of the pyroclastic deposit on the basin floor, freshly excavated impact materials, and peak ring material (see Section 6). These features were deemed to be targets of high scientific value based on the stated science objectives. Thus, a landing site was selected within roving distance of all three of these features in a region with less than 10° of slope and no observable obstacles in the $\sim 0.5\text{--}1 \text{ m pixel}^{-1}$ NAC images, as well as a Diviner average rock abundance of $<1\%$. The proposed nominal traverse totals 54 km in length and includes 12 individual stops, with several optional stops at potential features of interest included along the route. These stops were chosen in order to incorporate as many workshop-derived points of interest as possible, favoring those indicated as high-value targets during supplemental analysis. Individual stops were also selected to ensure the

observation and sampling of a range of different morphologic unit materials that would answer questions pertaining to each of the four main science goals. Details for each proposed stop are provided in Section 6. The chosen stops were then connected along traversable paths where LOLA-derived slope data show that there are no slopes of greater than 10° and both NAC images and the Diviner rock abundance map show that there are no obstacles that would prevent travel. Fortunately, the majority of the basin floor is flat lying and boulder free. The few boulders that were observed within the basin are generally clustered around easily identifiable geological features such as impact craters and debris falls associated with the peak ring. For additional details on the proposed traverse plan, see Section 6 below.

4. Mapping and Unit Descriptions

4.1. Morphologic Mapping

In contrast with the previous efforts discussed above, this study does not attempt to cover the entire basin. Based on our preliminary analysis and the results of the workshop, the northeastern basin floor associated with a portion of the central peak was identified as the primary region of interest for detailed mapping. The map presented in this work allows us to identify morphologically distinct units in greater detail at a smaller mapping scale compared to previous works within the identified region containing the greatest amount of scientifically valuable SOIs. For the main geomorphologic map of the northeastern half of the basin floor and central peak ring (Figure 3), eight morphologic units and major features were identified. Three additional small-scale units are included in the inset morphologic map of the area immediately surrounding the proposed landing ellipse. All 11 units were combined to form a morphologic map of the Schrödinger basin interior (Figures 3 and 4). This main map and all included images of the lunar surface are presented as simple

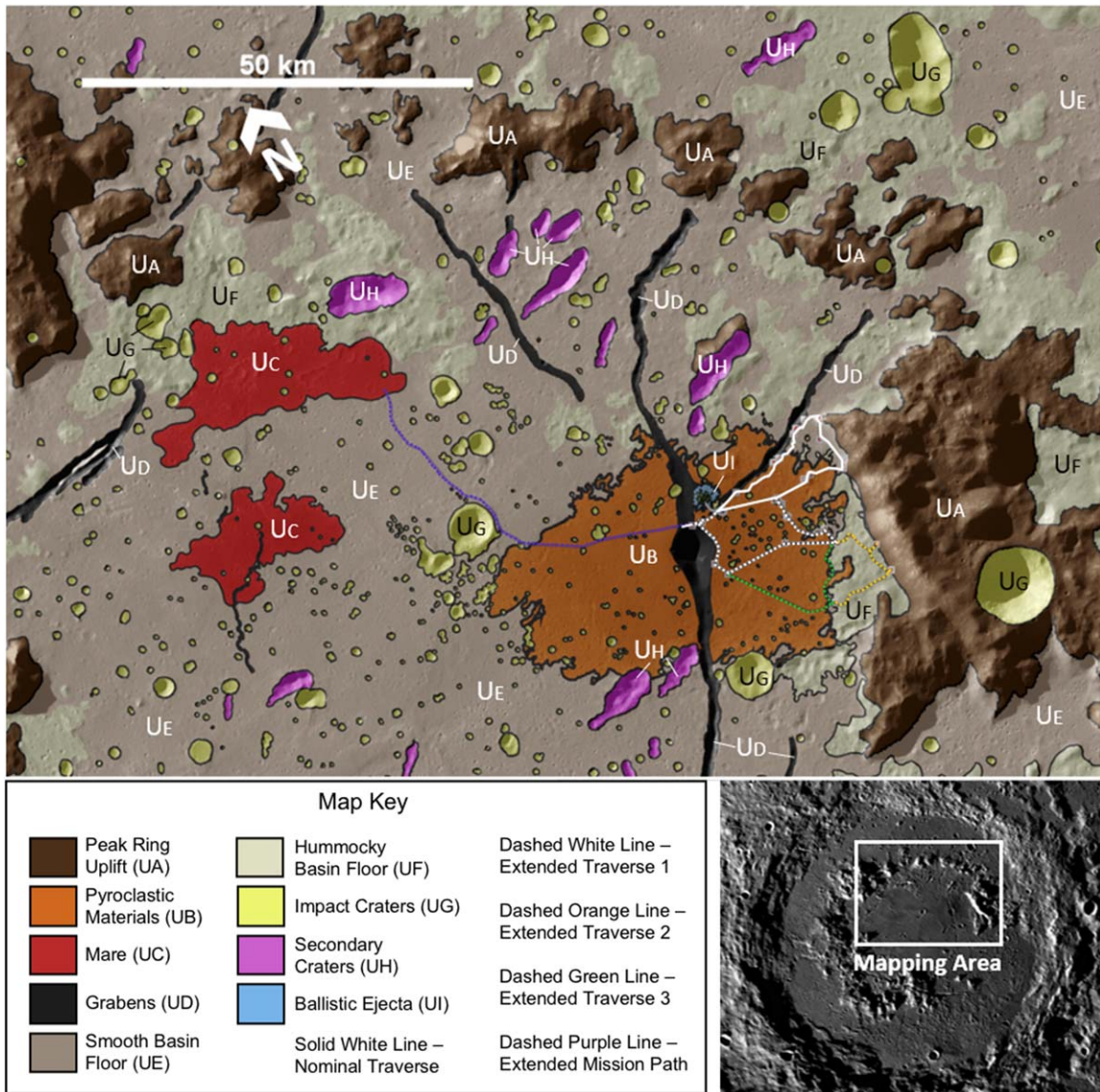


Figure 3. New morphologic map of the Schrödinger basin interior. All units are mapped as indicated in the included map key. The solid white line represents nominal rover traverse, the dashed green and orange lines represent optional extended rover traverse paths, and the purple dashed line represents the potential extended mission rover traverse path. Base image LROC-WAC mosaic. Simple cylindrical map projection used. Base Image Credit: NASA/GSFC/ASU.

cylindrical map projections. Further details about each of these mapped units are provided below and summarized in Figure 5.

A cover a total of 2500 km^2 within the mapped region, or 17% of the total mapped area.

4.2. Unit A—Raised Topography Surrounding the Central Basin Floor

The discontinuous ring of elevated topography near the middle of the basin is mapped here as Unit A (Figure 3). This unit consists of large coherent uplifted blocks of material that rise abruptly from the basin floor. These units reach elevations of up to ~ 3 km from the basin floor and have steeply sloping sides at the outer edges. The average slope for this mapped unit is 9° , with a maximum measured slope of 54.8° . At several locations along the base of this unit, material can be observed to have fallen down these slopes as debris falls. Several of these deposits have distinct boulder trails that are traceable up the slopes, indicating the point of origin among the elevated terrain for the fallen materials (Figure 6). The mapped deposits of Unit

4.3. Units B and C—Tonally Dark Regions

Near the center of the basin there are three distinct dark-toned units denoted here as Units B and C. Unit B consists of a single deposit centered at approximately $(138.92^\circ \text{ E}, -75.26^\circ \text{ N})$ covering a total surface area of $\sim 1035 \text{ km}^2$ (Figure 7). Unit C consists of two deposits centered at $(136.43^\circ \text{ E}, -73.47^\circ \text{ N})$ and $(134.54^\circ \text{ E}, -73.92^\circ \text{ N})$ (Figure 7). These two deposits cover a total surface area of $\sim 450 \text{ km}^2$. Both Units B and C consist of materials that are visibly darker in tonality than the surrounding basin floor materials. Units B and C feature flat surfaces, with little change in slope throughout. The average slope measured within the boundary of Unit B is 2.4° , and the average slope measured within the bounds of the deposits of Unit C is 1.2° . Furthermore, both Units B and C show significantly higher FeO abundance compared to the

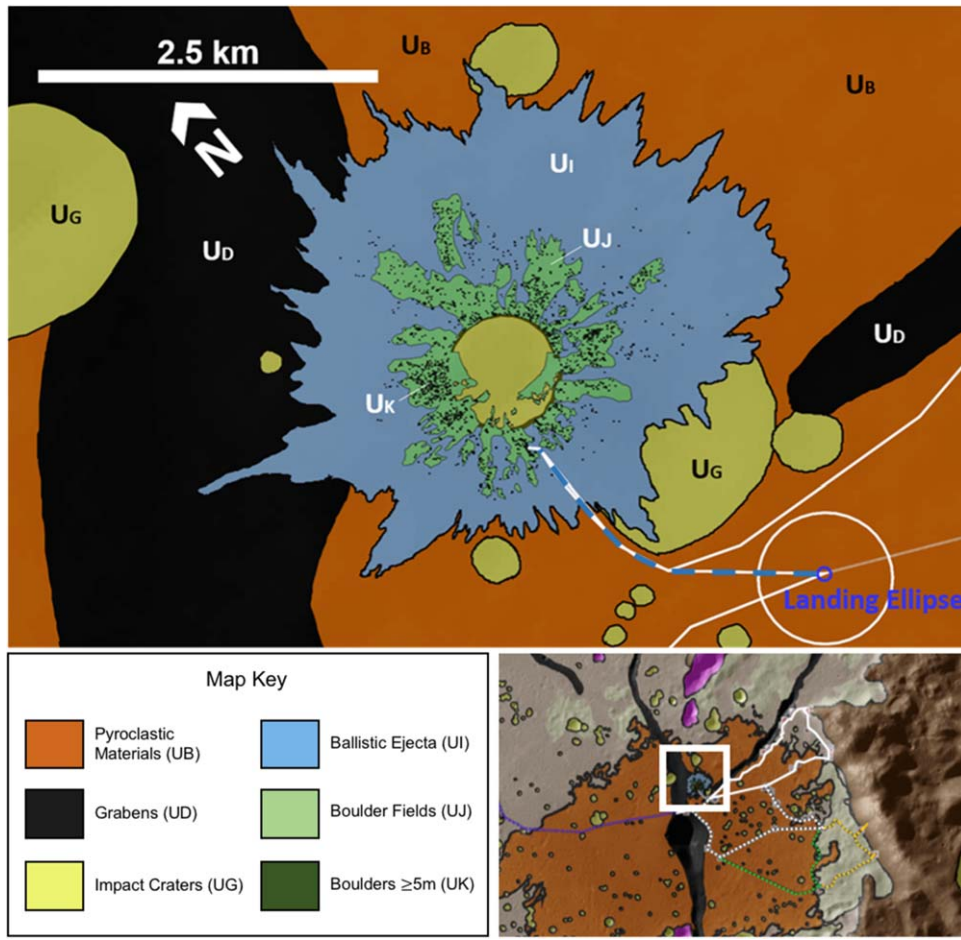


Figure 4. Morphologic map of landing ellipse and surrounding region. All morphologic units are mapped as indicated in the included map key. “Boulders >5 m” are individual boulders resolved in the $\sim 0.5\text{--}1$ m pixel $^{-1}$ NAC images. Each of these boulders is mapped as a distinct dark-green unit. “Boulder fields” are regions with multiple boulders <5 m in scale and a Diviner average rock abundance $\geq 4\%$. The size of the individual boulders makes them too small to map using the NAC images, but they collectively represent an impassable region for a rover. The white rectangle on the inset represents mapped area in context with the larger morphologic map (Figure 3). The blue circle represents the proposed 100 m landing ellipse. The white circle represents the wider 1 km threshold landing region. The white line represents the nominal rover traverse path. The dashed blue line represents the initial threshold traverse path. Simple cylindrical map projection used. Base image: LROC-WAC mosaic. Base Image Credit: NASA/GSFC/ASU.

surrounding basin materials in the Clementine spectral mapping data. The main difference between these units, and the reason we have separated them into two distinct morphologic units, is the different manner in which they interact with preexisting topography. Unit B surrounds a prominent linear depression with a wider elliptical depression at the center of the deposit (Figure 7). From this central point Unit B material is observed to drape the surrounding region and all preexisting topographic features with a layer of dark material that is thin enough to allow small preexisting topographic details to still be visible (Figure 7(A)). In contrast, the deposits of Unit C are observed to have collected in local topographic lows and embayed higher topographic features with a layer of material that is thick enough to have completely overprinted smaller topographic features.

4.4. Unit D—Elongated Linear Topographic Depressions

Unit D identifies the extent of a network of long linear depressions that run throughout the central basin floor. These depressions range from ~ 5 to 300 m in depth and vary in width from ~ 800 m to 5.5 km. These features have steeply sloping walls and flat-lying floors. The features of Unit D appear to

roughly follow two trends in orientation, either radial to the basin center or concentric with the peak ring and basin rim (Figure 1). These patterns in the distribution of these topographic depressions are also noted by Shoemaker et al. (1994). Several of these depressions do split or branch into multiple parallel or perpendicular depressions at distinct intersection points (Figure 8). The Unit D features cover a total surface area of 436.7 km 2 within the mapped region, or 3% of the total mapped area. As prominent features within the basin, these units are included in several previous maps of the region (Shoemaker et al. 1994; Mest 2011; Kramer et al. 2013; Shankar et al. 2013).

4.5. Units E and F—Basin Floor

We have divided the basin floor into two distinct units. Unit E represents regions of the basin floor that are observed to be smooth flat-surfaced plains, with the only significant topographic features attributed to the occurrence of intermittent post-Schrödinger impact structures (Unit G) or long linear depressions (Unit D) (Figures 9(A) and (B)). Within Unit E the average measured slope is 1.96°. Unit E covers a total surface area of 2800 km 2 . Unit F represents portions of the basin floor

Unit Name	Color on Map	Total Surface Area Mapped	LOLA 1024 PPD Slope				Brief Description	Interpretation (This Study)
			Min.	Max.	Avg.	Std. Dev.		
Unit A		~2,500 km ²	0°	54.8°	9.0°	5.2°	Circular region of topographically high terrain with steeply sloping sides.	Central peak ring of Schrödinger Basin
Unit B		~1,040 km ²	0°	51.8°	2.4°	2.4°	Tonally dark unit that appears to be draping preexisting topography completely surrounding a central vent. Shows high wt. % FeO in Clementine UVVIS FeO abundance map.	Pyroclastic deposit
Unit C		~450 km ²	0°	42.9°	1.2°	1.2°	Dark-toned flat lying material approximating an equipotential surface covering the lowest portion of the crater interior. Shows high wt. % FeO in Clementine UVVIS FeO abundance map.	Post-impact mare deposits
Unit D		~440 km ²	0°	49.8°	5.2°	3.9°	Network of narrow steep-sided grooves in the basin floor. There appear to be two sets, one radial to the basin centre and one circumferential with the central peak ring.	Post-impact extensional grabens
Unit E		~2,800 km ²	0°	48.3°	2.0°	1.9°	Smooth, flat lying unit comprising portions of the present-day basin floor.	Portions of the interior impact melt sheet.
Unit F		~2,200 km ²	0°	71.7°	4.4°	3.3°	Hummocky (blocky) portions of the present-day crater floor. Predominantly expressed near the central peak ring structure.	A combination of crater fill materials and post-impact mass wasting debris from the central peak ring
Unit G		~800 km ²					Local topographically low features that are circular in overall shape, with slightly raised rims.	Post-Schrödinger impact craters
Unit H		~275 km ²					Elongated local topographically low features with slightly raised rims.	Secondary impact craters from large external post-Schrödinger impact events
Unit I		~9.3 km ²	0°	33.2°	3.8°	3.4°	Radially grooved terrain surrounding a small, well-preserved impact crater on the basin floor.	Continuous ballistic ejecta blanket
Unit J		~0.08 km ²	0°	32.8°	3.7°	2.2°	Collections of smaller coherent blocks of material < 5 m across.	Small rock and boulder fields ejected from the small impact crater
Unit K		~0.04 km ²					Individual coherent blocks of material >5 m across.	Large boulders ejected from the small impact crater

Figure 5. Summary and measurements for the mapped units within Schrödinger basin.

that are composed of blocky or hummocky terrain. Within these regions the average measured slope is 4.39°. Unit F is observed throughout the central basin region but is found in greatest concentration near the base of the central peak ring (Figures 9(C) and (D)). The basin floor regions between the discontinuous blocks of peak ring material are observed to be composed of mostly Unit F material. Unit F covers a total surface area of 2180 km², or 15% of the total mapped area.

4.6. Units G and H—Local Topographic Depressions

Throughout the mapped region, post-Schrödinger impact craters >20 m in diameter are identified as Unit G (Figure 10). These craters are identified as round to subround topographic depressions in the surrounding terrain with slightly elevated topographic rims. The features of this unit are observed to

overprint all other identified units in the regional map. Unit G consists of only individual topographic depressions. Unit H is identified as linear chains of multiple round to oval-shaped topographic depressions with slightly raised rims that overlap or occur directly adjacent to one another (Figure 10). Many of these Unit H features are observed to parallel one another, extending in a northeast—southwest direction.

4.7. Unit I—Radially Grooved Terrain

The inset morphologic map (Figure 4) features several additional units in the immediate vicinity of the proposed landing site that are only discernible at this smaller scale. The surface surrounding an unnamed 0.9 km diameter well-preserved impact crater to the north of the landing ellipse is observed to host a pattern of curvilinear grooves oriented

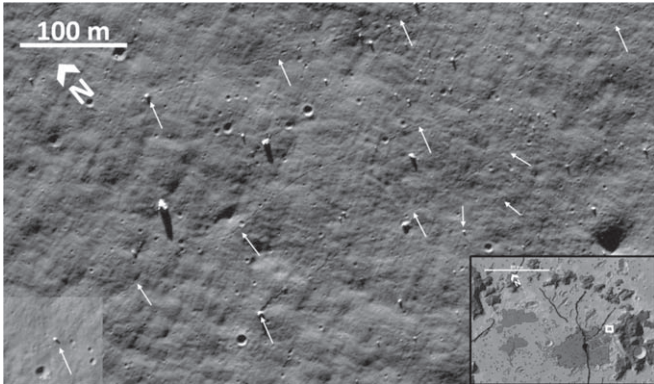


Figure 6. LROC-NAC image of four distinct boulder trails extending down the interior slope of the Schrödinger peak ring. Each of these trails is indicated by the white arrows. The location relative to the rest of the Schrödinger basin interior is indicated by the white box on the inset map. Base Image Credit: NASA/GSFC/ASU.

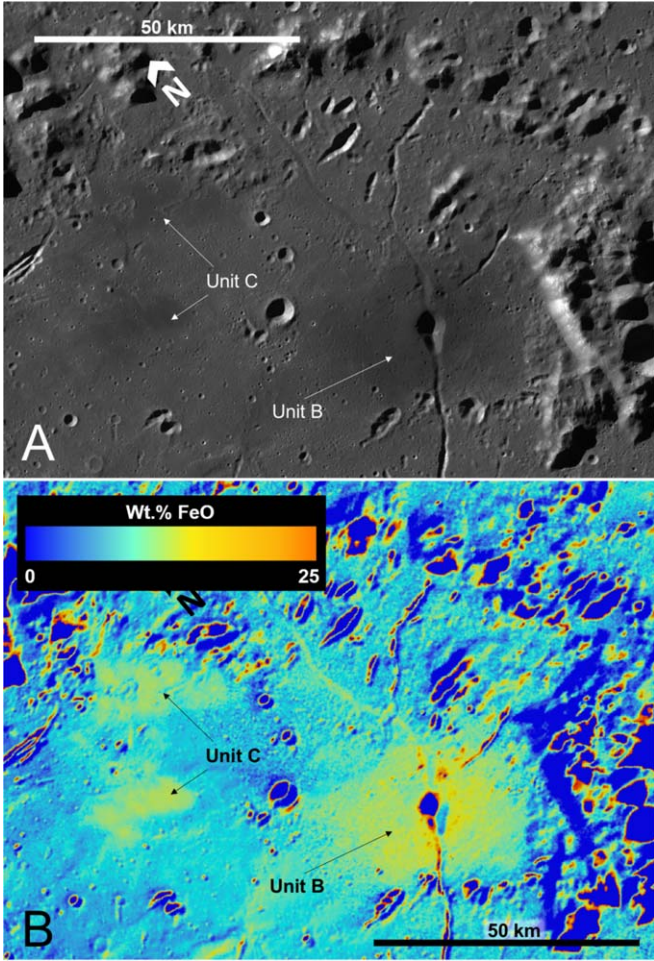


Figure 7. (A) LROC-WAC image of the interior basin floor. Three distinct patches can be observed in this image labeled Unit B to the right and two labeled Unit C to the left. A large topographic depression can be observed at the center of the Unit B deposit. (B) Same perspective overlaid with the Clementine FeO abundance map. These three units can each be observed to have a significantly higher FeO abundance than the surrounding basin units. Base Image Credit: NASA/GSFC/ASU.

radially to the crater center. This unit completely surrounds the crater in all directions and extends from the crater rim to ~ 0.8 km to the south and ~ 2 km to the north. This unit has a

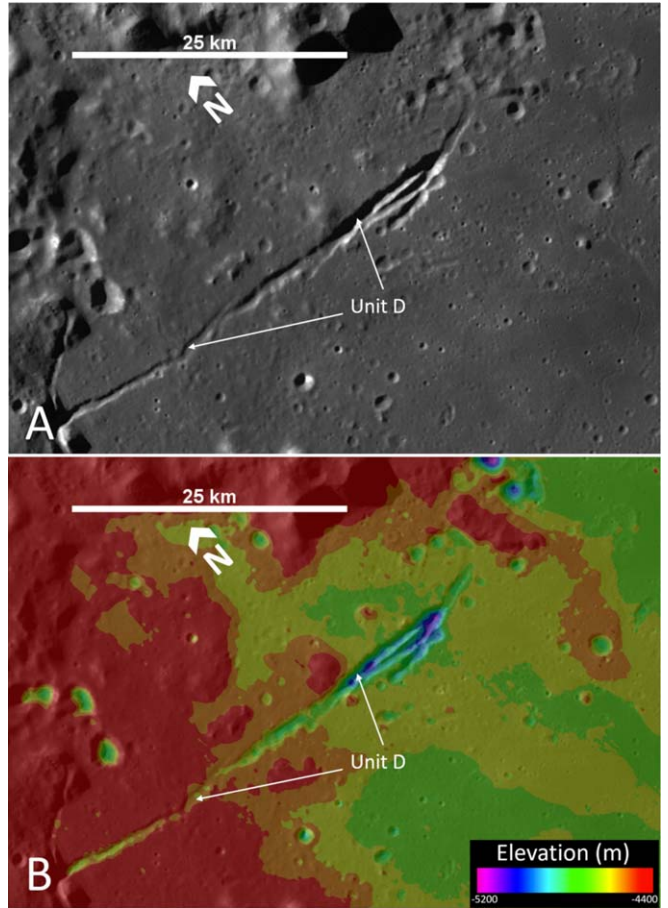


Figure 8. (A) LROC-WAC image of the flat-lying interior basin floor illustrating the elongated linear negative topographic features identified here as Unit D. (B) Same perspective overlaid with LOLA 1024 PPD elevation data colorized as indicated in the inset key in order to better illustrate the change in topography in the basin floor associated with the features of Unit D. Base image: LROC-WAC mosaic. Base Image Credit: NASA/GSFC/ASU.

significantly higher CPR value than the surrounding lunar surface terrain (Figure 11). Unit I material is also observed to overprint preexisting topographic features such as older impact structures. Unit I has an average slope of 3.7° and covers a total surface area of 9.3 km^2 .

4.8. Units J and K—Small Blocks and Block Clusters

There are two additional units of material situated near the rim of this same small, well-preserved impact crater to the north of the proposed landing site (Figures 11 and 12). Lobate clusters of blocks and rugged terrain are observed concentrated at the crater rim and extending both into the crater and out onto the exterior lunar surface beyond the rim (Figure 12). These fields contain numerous coherent blocks of material varying from <1 to ~ 20 m in size. Here we identify the fields of smaller blocks as Unit J and map individual blocks 5 m and larger as Unit K. Deposits of both Units J and K are observed to be evenly distributed around the crater and extend outward in all directions from the crater rim. Both Units J and K reach maximum radial distances of up to 0.8 km from the crater rim. Collectively deposits of Units J and K cover a total surface area of $\sim 1.3 \text{ km}^2$.

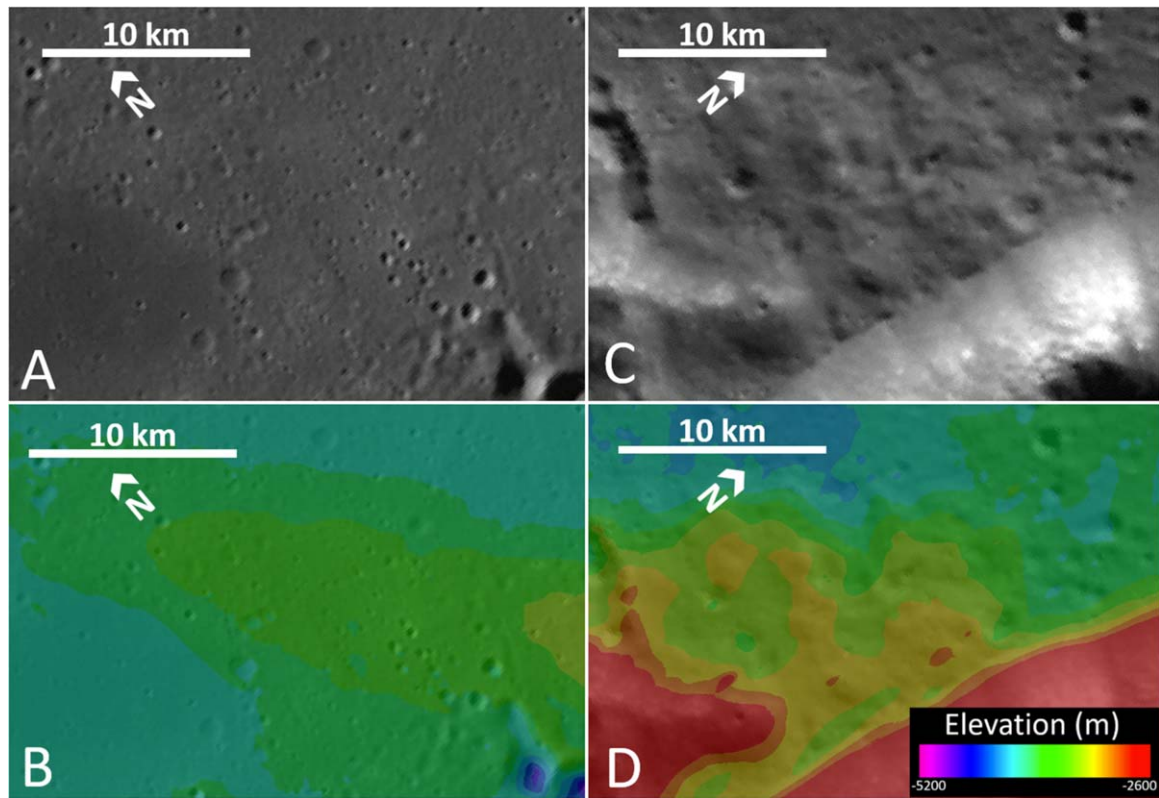


Figure 9. (A) LROC-WAC image of the smooth flat-surfaced basin floor identified here as Unit E. (B) Same perspective overlain with LOLA 1024 PPD elevation data to better illustrate the subtle changes in topography throughout this unit. (C) LROC-WAC image of the hummocky basin floor identified here as Unit F. (D) Same perspective overlain with LOLA 1024 PPD elevation data to better illustrate the more abundant changes in topography throughout this unit compared to Unit E. Base image LROC-WAC mosaic. Elevation images are colorized as indicated in the inset key. Base Image Credit: NASA/GSFC/ASU.

5. Unit Interpretations

5.1. Unit A—Peak Ring Material

Due to the overall circular grouping of the features of Unit A and the presence of such steeply sloping elevated terrain near the center of the otherwise flat-lying basin floor, we interpret this unit as the uplifted peak ring of Schrödinger. This interpretation is consistent with previous analyses of the Schrödinger basin interior (Mest 2011; Kramer et al. 2013). Kring et al. (2016) suggested that the peak ring material was likely uplifted as much as 30 km from depth. This would make the peak ring unit the most probable host for materials that formed prior to the Schrödinger basin impact, including SPA materials. Thus, sampling Unit A is important for science goals 1 and 2: better understanding impact cratering processes in how central uplifts form, and lunar chronology, for the potential dating of uplifted ancient lunar material. While the steep slopes of Unit A would prevent a rover from ascending the elevated terrain to sample the peak ring directly, numerous boulder tracks have been identified (Figure 6), which have brought peak ring materials down to the inner basin floor. These boulder falls, especially those with discernible boulder trails extending up the slope to the origin point of the rock fall, are viewed as highly desirable sampling targets for the rover platform and have been included in both the nominal and extended rover traverses discussed below. These boulder targets are comparable in scale and potential scientific value to the Station 6 boulder sampled during the Apollo 17 mission.

5.2. Units B and C—Volcanic Deposits

The relatively high FeO abundance compared to the surrounding crater materials and the dark-toned appearance of these units in the visible images both indicate that the deposits of Units B and C are volcanic in origin. However, the interaction of these units with the preexisting topography indicates different emplacement mechanisms for Units B and C. Unit B is observed to exist as a thin layer of material covering all surrounding preexisting topographic features surrounding a central topographic depression. We interpret this unit as a pyroclastic deposit. This interpretation is consistent with previous observations and mapping efforts covering the Schrödinger basin floor (Shoemaker et al. 1994; Mest 2011; Kramer et al. 2013). These previous works each interpret the large oval-shaped depression near the center of this unit to be the vent from which this material originated. Pyroclastic or fire fountaining deposition from a central vent would explain the manner in which this material coats the surrounding terrain (Rutherford & Papale 2009; Wetzel et al. 2015). Pyroclastic volcanism on Earth requires the presence of volatile material to produce the fire fountaining effect. This indicates that the pyroclastic deposit on the floor of Schrödinger basin (Unit B) may contain trace amounts of volatile material, including water, which would be a valuable in situ resource for future crewed surface exploration missions (Kring et al. 2014). Several studies have identified trace amounts of volatile materials within lunar volcanic glass beads collected during the Apollo missions to the lunar surface (e.g., Saal et al. 2008; McCubbin et al. 2015). Considering that at most only trace amounts of volatile material would likely be

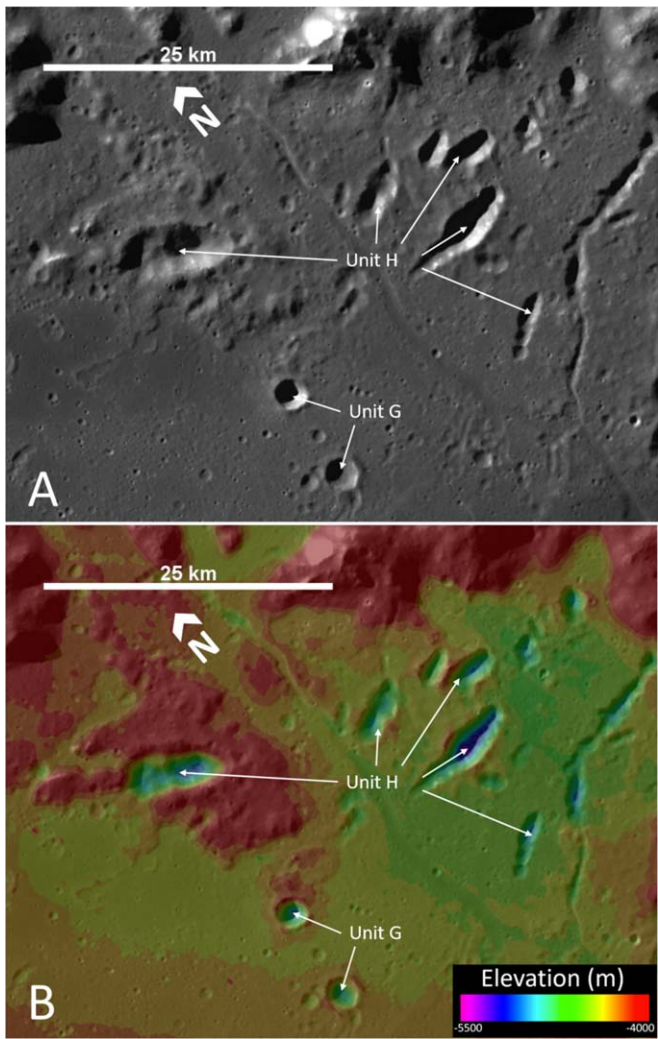


Figure 10. (A) LROC-WAC image of several post-Schrödinger impact structures observed as local topographic low features in the otherwise flat-lying basin floor. Individual impacts are observed as circular depressions in the basin floor and are labeled here as Unit G. Elongated elliptical impacts or chains of craters are identified here as Unit H. (B) Same perspective overlaid with LOLA 1024 PPD elevation data to better illustrate these topographic depressions in the basin floor. Elevation data are colorized as indicated in the inset key. Base image: LROC-WAC mosaic. Base Image Credit: NASA/GSFC/ASU.

present in the pyroclastic deposit within Schrödinger, this location is primarily considered a target for scientific investigation of lunar volatiles rather than a proposed location for resource extraction. It is also possible that this deposit of pyroclastic material may contain mantle xenoliths that were transported from the lunar interior during the pyroclastic eruption. If found, these mantle xenoliths could provide insight into the composition of the lunar mantle and timing of the lunar mantle formation (Kring 2013; Steenstra et al. 2016). Thus, the pyroclastic deposit is the highest-priority unit for sampling during the proposed traverse, as it could address three out of four of the main science goals: lunar chronology, lunar volcanism, and represents a potential in situ resource for future manned missions to the lunar surface. The proposed traverse presented below includes several sampling points at different locations throughout this unit in order to thoroughly assess the composition and volatile content of this unit.

Unit C is also observed to have filled local topographic lows with iron-rich, dark-toned material to form flat-lying smooth

surfaced units. This is consistent with the formation and appearance of infilled mare deposits on the lunar surface (e.g., Wilhelms et al. 1987; Head & Wilson 1992). We therefore interpret Unit C to be infilled mare deposits that occurred after the formation of Schrödinger basin. Several previous studies that included this region of the Schrödinger basin floor also mapped and interpreted these features as mare deposits (Shoemaker et al. 1994; Mest 2011; Kramer et al. 2013; Shankar et al. 2013). These mare deposits represent a moderately high priority target for the originally proposed HERACLES rover mission, as they would address two of the four science goals: lunar chronology and lunar volcanism.

5.3. Unit D—Basin Floor Grabens

The long curvilinear nature of these topographic depressions paired with the steep slopes of the interior walls and flat-lying floor led us to interpret the features of Unit D as a network of extensional grabens cutting throughout the basin floor. Shoemaker et al. (1994) suggest that these grabens likely formed owing to a slight uplift of the basin floor caused by isostatic rebound following the emplacement of the impact melt sheet at the end of the formation of Schrödinger. This theory is supported by the overall ring-shaped pattern of these grabens, which would be indicative of this type of local rebound and extension (Schultz 1976; Shoemaker et al. 1994). These grabens are prominent topographic features running through the central basin floor and as such have been included in several previous maps and morphologic interpretations of the Schrödinger basin region (Shoemaker et al. 1994; Mest 2011; Kramer et al. 2013; Shankar et al. 2013). The steep slopes of these features render them a navigational obstacle and a potential hazard for a rover platform that must be considered when plotting the proposed traverse.

5.4. Units E and F—Basin Floor Impactite Materials

In this morphologic mapping we have divided the basin floor into two units based on expressed texture. The majority of the basin floor is smooth and flat lying. We have included these regions as Unit E. This material is interpreted to be the remainder of the impact melt sheet and other impactites that formed as a result of the Schrödinger impact event. The Unit E material would have covered the topographically low basin floor as a coherent melt sheet (e.g., Oberbeck 1975; Melosh 1989; Osinski et al. 2011, 2018). This surface material has since been reduced to regolith by ~ 3.8 Gyr of subsequent impact gardening (Shoemaker et al. 1994; Shankar et al. 2013). The remainder of the basin floor is hummocky to blocky and labeled as Unit F. Based on the proximity of Unit F materials to peak ring materials (Unit A), we interpret Unit F materials to be a mixture of material from the Schrödinger basin interior melt sheet and solid basin-fill materials, including rock falls, landslides, and collapsed peak ring materials that fell, spread out over portions of the basin floor, and were subsequently draped by impact melt. The exact timing of emplacement for these materials is unclear, but it likely began during the modification stage, with the majority of materials emplaced shortly after the end stages of the impact cratering process. While hummocky in appearance, the surface of Unit F is contiguous with that of Unit E in most locations. It is possible that this contiguous contact is the result of mixture of the basin-fill materials with the still molten melt sheet early in the impact cratering process. However, it is more

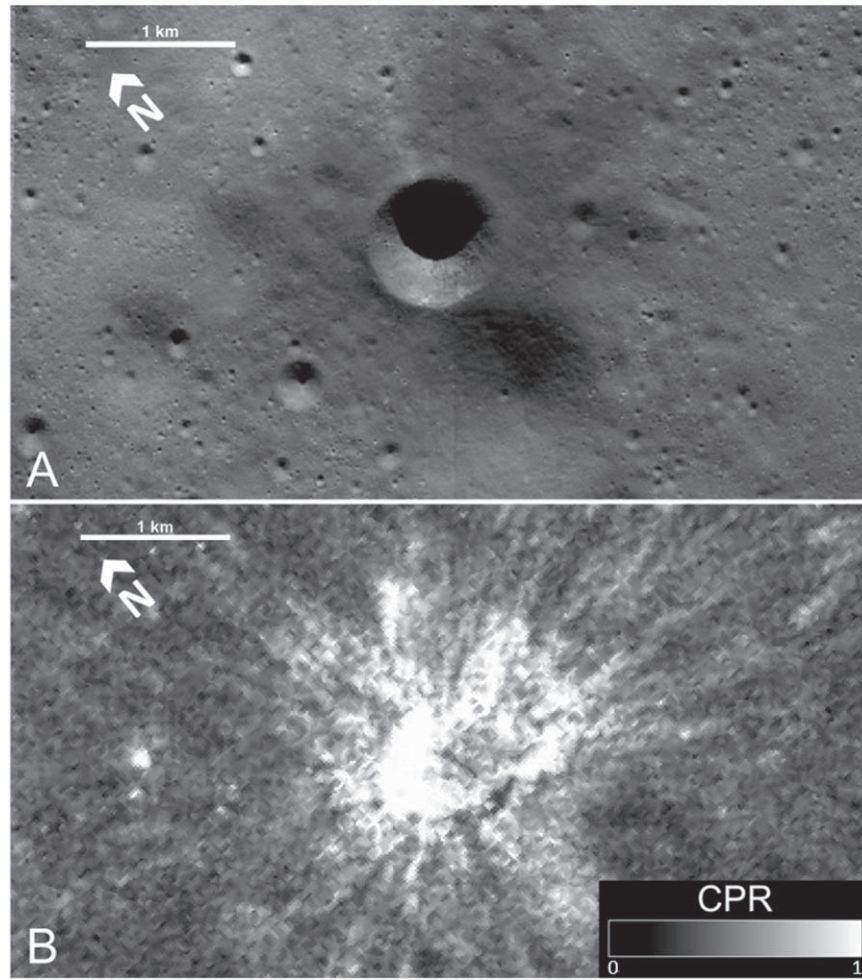


Figure 11. (A) Small unnamed impact into the Schrödinger basin floor. This impact is better preserved than other impact structures of the same size in the region. A distinct radial surface pattern can be observed surrounding this crater and is identified here as Unit I. (B) Same perspective overlain with Mini-RF CPR Radar data. Bright white pixels indicate a CPR of 1, while black pixels represent a CPR of 0. CPR values of 1 indicate a rough surface texture on the order of ~ 10 cm. This rough surface material corresponds to the same region as the radial grooved texture observed above. Base Image Credit: NASA/GSFC/ASU.

likely that this smooth transition between the deposits of Units E and F is due to the result of billions of years of impact gardening smoothing out the contact between the two units and eroding the constituent material of both types of deposit into a fine regolith. One deposit of Unit F material, located near the western edge of the pyroclastic deposit (Unit B), is within reach of the rover platform from the proposed landing site. This deposit of Unit F materials is expressed as a lobate landform of hummocky to blocky terrain that hugs the inner peak ring wall. As these deposits of Unit F likely contain significant amounts of uplifted peak ring materials, visiting this deposit would enable the sampling of materials that potentially address science goals 1 and 2: impact cratering processes and lunar chronology. There is a distinct line of transition from the smooth flat-lying deposits on the basin floor to the topographically elevated deposits of Unit F. The rugged surface features of Unit F would likely prove to be difficult or impossible to navigate with the rover platform. Thus, potential samples from within this unit are included in the extended sample traverse plan detailed below.

5.5. Units G and H—Post-Schrödinger Impact Craters

All circular depressions within the mapping region greater than 20 m in diameter that feature slightly raised rims and bowl-shaped interiors are interpreted as impact craters that

post-date the formation of Schrödinger basin. These are mapped and discussed here as Unit G. These units are of moderate interest when planning the rover traverse path, as their formation excavates material from depth, providing easy access to materials the rover platform would otherwise be unable to access. As such, excavated materials from relatively fresh small impact craters of Unit G could potentially answer questions related to science goals 1 and 2: impact cratering processes and lunar chronology. The large topographic depression at the center of the pyroclastic deposit (Unit B) is excluded from the group of features identified here as Unit G. The position of this particular feature along an extended graben paired with the surrounding pyroclastic material has led to the interpretation of this topographic depression as a volcanic vent rather than an impact crater.

Additionally, the elongated elliptical depressions with raised rims that are not associated with any of the extensional grabens or observable volcanic deposits are included as Unit H. These features are interpreted as secondary impact craters from large craters external to Schrödinger. Shoemaker et al. (1994) attribute several of these crater chains to the Antoniadi, Humboldt, and Orientale impact events. Kramer et al. (2013) state that secondary crater features within Schrödinger basin originate from as many as seven separate external impact-

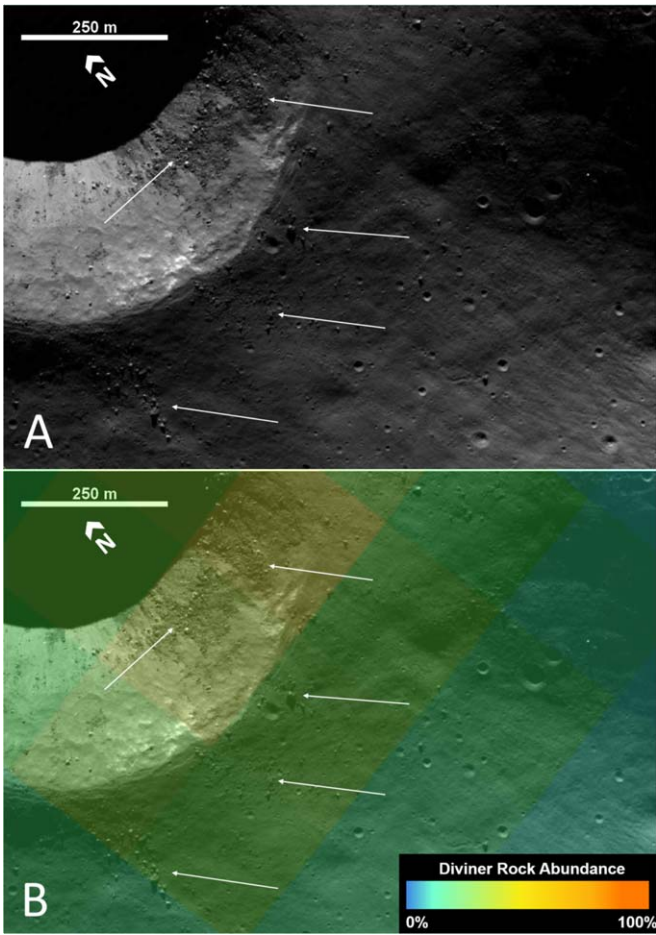


Figure 12. (A) LROC-NAC image (M128385314LC) illustrating the blocky units surrounding the small, well-preserved impact identified above. White arrows indicate clusters of blocks (Units J and K) on and around the crater rim. (B) Same image overlaid with Diviner rock abundance data colorized as indicated in the inset key. Base Image Credit: NASA/GSFC/ASU.

forming events, including Tsiolkovsky, Lyman, Antoniadi, Orientale, Hausen, Hale, and Humboldt craters. These previous interpretations are primarily based on the radial orientation of these observed secondary impact crater chains to the proposed host craters. For the map presented in this paper, we do not attribute these secondary crater features to any particular external impact event, but note that there are no intra-Schrödinger potential source craters. Further in situ analysis of these features could indicate whether there is potential for sampling additional geologic materials from outside of Schrödinger or for dating the primary impact structures that generated the secondary craters found in Schrödinger. For future rover missions to the region, the features of Unit H are of equal interest to the features of Unit G, as both provide an opportunity to observe and sample excavated lunar materials.

5.6. Unit I—Continuous Ballistic Ejecta Blanket

Unit I completely surrounds the small, well-preserved impact crater to the north of the proposed landing zone as shown in the inset map (Figure 4). Due to the location of this unit and the morphologic characteristics described above, including the radial grooves and high degree of surface roughness, we interpret this unit as the continuous ballistic ejecta blanket of the small, unnamed crater. These ejecta materials are extremely

well preserved and overprint the surrounding pyroclastic deposits, indicating that the emplacement of Unit I postdates the deposition of the volcanic materials. Unit I likely hosts materials that have been excavated from both the pyroclastic layer and the pre-pyroclastic lunar surface beneath. Thus, these ejecta deposits likely represent a combination of pyroclastic and basin floor materials that have been exposed to conditions on the lunar surface for the least amount of time of any such materials found within the proposed study region. The ejecta materials of Unit I would likely produce well-preserved samples of pyroclastic and basin floor material from depth and are thus a high priority for sampling during the proposed rover traverse. However, given the high degree of surface roughness as observed by Mini-RF CPR (Figure 11(B)), this region may be difficult or impossible to traverse safely with the rover platform. Additional navigational information, including in situ images and LIDAR scans, would be needed in order to determine whether Unit I is safe to traverse.

5.7. Units J and K—Boulders and Boulder Fields

Based on the distribution of the features of Units J and K around the rim of the small, well-preserved, 0.9 km diameter impact crater north of the proposed landing site (Figures 4 and 11), the blocks of solid material are interpreted to be excavated boulders that originated from within the crater itself. These blocks would have been ejected on ballistic trajectories during the early stages of crater formation, traveling above the lunar surface and coming to rest at or near the crater rim (e.g., Oberbeck 1975; Melosh 1989). We have denoted all blocks greater than 5 m across as Unit J, and all fields of smaller boulders have been mapped together as Unit K. All of these blocks likely represent pieces of the Schrödinger basin floor that have been exposed to lunar surface conditions for a relatively short amount of time. Thus, they represent opportunities to sample preserved floor material from depth with the rover platform, addressing science goals 1 and 2: impact cratering processes and lunar chronology. Several individual boulders have been identified as potential sampling targets for the proposed traverse, as they are situated near relatively flat terrain and should be accessible to the rover platform.

6. Rover Traverse Plan and Concept of Operations

Three variations of the traverse were produced: a *threshold* traverse (represented by the blue dashed line in Figures 4 and 13), a *nominal* traverse (represented by the solid white line in Figures 3 and 13), and an *extended* traverse (represented by the white, green, and orange dashed lines in Figures 3 and 13). Each of these segments reflects the progress toward completing the overall mission goals accomplished by that segment of the rover traverse. The threshold traverse meets the minimum requirements for a successful mission with a short distance traveled and one sample obtained. The nominal traverse includes the threshold traverse as part of the full proposed 54 km distance and enables sampling at up to 12 locations, which would meet all main science goals for the mission (Figure 13). The extended traverse paths are far longer and incorporate additional sampling locations that would provide additional context to the geology of Schrödinger basin but are not critical to obtain if similar samples are acquired during the nominal traverse. These extended options are included as possible options for an extended mission scenario. Each of these

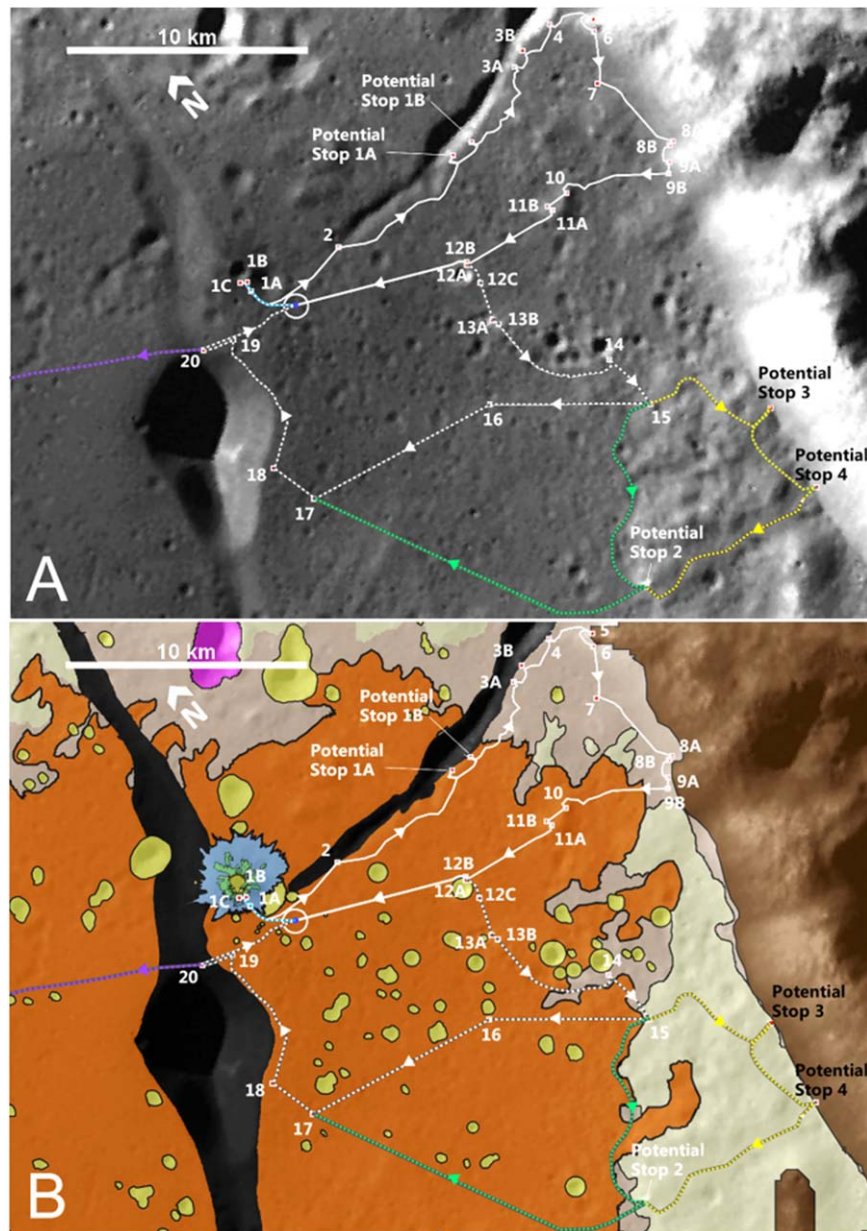


Figure 13. (A) LROC-WAC image of the proposed rover traverse path. The nominal 100 m diameter landing ellipse is indicated by the dark-blue circle. The threshold 1 km landing ellipse is indicated by the white circle. The threshold 5.2 km traverse is indicated by the dashed blue line. The nominal 54 km traverse is indicated by the solid white line. Potential extended traverse paths are indicated by the white, orange, and green dashed lines. The potential extended mission traverse to additional basin floor locations is indicated by the purple dashed line. The direction of travel on all traverse paths is indicated by the arrows along each path. Each stop is indicated by a red point and numbered accordingly. (B) Same perspective overlaid with our mapped units to better illustrate the surface materials present at each stop and along each leg of the proposed traverse path. Base image: LROC-WAC mosaic. Base Image Credit: NASA/GSFC/ASU.

traverse segments is discussed in greater detail in the following sections.

6.1. Proposed Landing Site

We identified a 100 m diameter landing ellipse, centered at (140.071° E, -75.235° N), as specified by the initial HERACLES constraints. This landing ellipse is shown in blue on the basin floor morphologic overview and inset maps. Additionally, a 1 km diameter threshold landing region is denoted as a white circle. Based on remote sensing data analysis, this entire region appears to be flat lying (<10° of slope) and with no boulders visible in the ~0.5–1 m pixel⁻¹ NAC images and a Diviner average rock abundance of <1%, making it safe for landing. The 1 km zone

around the proposed landing ellipse also represents a region that would be most significantly affected by the lander's descent thrusters on approach to the lunar surface based on analysis of the Apollo landing sites (e.g., Clegg et al. 2014), as well as recent modeling of lander exhaust (Prem et al. 2020). This means that any sampling of lunar material should take place outside this zone to avoid sampling materials that are contaminated or altered by the descent vehicle during the landing process.

6.2. Threshold Traverse

The proposed traverse begins with a northward drive toward the rim of a small, well-preserved, 0.9 km diameter crater located nearby. We identified three potential stops within the

*Stop Number	Latitude	Longitude	PHASR Science Goals				Brief Site Description
			Lunar Volcanism	Lunar Chronology	Impact Cratering Processes	Human Habitability	
Stop 1A	-75.18192	139.94191			X	X	Boulder field associated with fresh impact into the pyroclastic materials.
Stop 1B	-75.16858	139.95862	X				
Stop 1C	-75.16237	139.92708					
Stop 2	-75.21214	140.4527	X	X			Boulders situated near the edge of a large floor graben within the pyroclastic deposit.
Stop 3A	-75.17305	141.80883	X	X			Boulder field situated on the edge of a floor graben.
Stop 3B	-75.16218	141.89871					
Stop 4	-75.15681	142.10173	X	X			Boulder field situated on the edge of a floor graben.
Stop 5	-75.18835	142.3011		X	X		Boulder field with clearly observable boulder trails indicating that the materials originated from higher elevation within the peak ring.
Stop 6	-75.2027	142.26038		X	X		Boulder field with clearly observable boulder trails indicating that the materials originated from higher elevation within the peak ring.
Stop 7	-75.26206	142.09687		X	X		Regolith sample site due to strong olivine signature in orbital compositional data. Potential landslide or flow features observed at this location.
Stop 8A	-75.38977	142.2167		X	X		Boulder field with clearly observable boulder trails indicating that the materials originated from higher elevation within the peak ring. Potential anorthosite signature at this location as well.
Stop 8B	-75.39093	142.18993					
Stop 9A	-75.42153	142.08659		X	X		Boulder field at the base of the peak ring. Potential anorthosite signature at this location as well.
Stop 9B	-75.40974	142.12546					
Stop 10	-75.35445	141.58801		X			Boulders and potential in-situ outcrop; material does not appear to have originated in the peak ring, may be locally sourced.
Stop 11A	-75.36082	141.46959	X	X			Two small well-preserved craters into the pyroclastic material. Potential for sampling excavated pyroclastic material from depth.
Stop 11B	-75.35261	141.46201					
Stop 12A	-75.34242	140.85538					Boulders near the rim of a well-preserved crater located at the outer edge of the continuous pyroclastic deposit. Potential to sample pre-pyroclastic surface material from depth.
Stop 12B	-75.345	140.91849	X		X		
Stop 12C	-75.37561	140.90955					
Stop 13A	-75.42654	140.82778	X		X		Boulders near the rim of a well-preserved crater located at the outer edge of the continuous pyroclastic deposit. Potential to sample pre-pyroclastic surface material from depth.
Stop 13B	-75.43658	140.839					
Stop 14	-75.5715	141.17647	X				Boulder field situated on the edge of a local depression near the margin of the pyroclastic deposit. Potentially pre-pyroclastic basin floor material.
Stop 15	-75.6554	141.19205			X		Boulder field at the edge of the hummocky terrain. Navigational assessment point to determine if the hummocky terrain near the base of the peak ring is traversable.
Stop 16	-75.51432	140.51437	X			X	Stop along the long pyroclastic traverse. Possible regolith / pyroclastic sample to assess the diversity of pyroclastic materials at varying distances from the main vent.
Stop 17	-75.45555	139.44058	X			X	Stop along the long pyroclastic traverse. Possible regolith / pyroclastic sample to assess the diversity of pyroclastic materials at varying distances from the main vent.
Stop 18	-75.38653	139.38834	X			X	View point near the edge of the main vent. Stop to image the vent interior and obtain additional pyroclastic material from near the vent rim.
Stop 19	-75.21531	139.6938	X			X	View point near the edge of the main vent. Stop to image the vent interior and obtain additional pyroclastic material from near the vent rim. Also navigational assessment point for future extended mission traverse toward the mare material across the basin floor.
Stop 20	-75.19976	139.53626	X				View point near the edge of the main vent. Stop to image the vent interior and obtain additional pyroclastic material from near the vent rim.
Potential Stop 1A	-75.21469	141.24722					
Potential Stop 1B	-75.21657	141.37014	X	X			Boulder field along fissure. May expose impact melt materials associated with the Schrödinger impact. May be difficult to access due to sloping terrain.
Potential Stop 2	-75.84657	140.50242	X	X			Massive boulder field near the edge of the hummocky terrain.
Potential Stop 3	-75.7642	141.69249		X	X		Boulder field along the base of the peak ring. Some boulder trails visible.
Potential Stop 4	-75.88969	141.60771		X	X		Boulder field along the base of the peak ring. Some boulder trails visible.

Figure 14. Location and details for potential sampling locations along the proposed threshold, nominal, and extended Rover traverses.

ejecta blanket of this crater, stops 1a, 1b, and 1c, where there are abundant boulders and surrounding regolith for sampling (Figure 14). The rocks here were protected from the effects of space weathering in the subsurface, until they were excavated by the 0.9 km crater. These ejecta are likely composed of pyroclastic materials and potentially Schrödinger melt sheet material from beneath the pyroclastic layer. Sampling this

relatively fresh excavated material would provide further insight into the depth and composition of the pyroclastic deposits. After sampling and observations within the ejecta blanket are completed, the traverse path proceeds back past the landing site and continues further on toward the east. This initial path in and out of the ejecta blanket represents a threshold traverse distance of 5.2 km. Passing the lander in

route to the remaining stops provides an opportunity to return any samples collected thus far in the mission to the lander for transport to Earth if any major problems occur during the initial operational stages and the mission is forced to end early.

6.3. Nominal Traverse

The nominal traverse path includes the initial traverse into the ballistic ejecta blanket of the small, 0.9 km diameter crater and continues clockwise along the path indicated by the solid white line in Figure 13. This nominal path is a total of 54 km in length and accesses several additional units of surface materials compared to the threshold traverse. With a proposed average speed of 2 km hr^{-1} this traverse path divides the total 1130 hr of mission time into 27 hr of drive time and 1103 hr for science and engineering operations. If the total operational time is divided evenly between all SOIs along the nominal traverse, the rover could stop for a maximum of 52.5 hr at each proposed stop. Additionally, if the 2 km hr^{-1} driving speed proves too optimistic, there is still time in the mission plan to visit all the SOIs by reducing the time at each stop.

Stops 2, 3a, 3b, and 4, along with potential stops 1a and 1b, are all associated with a large graben running across the northern end of this nominal traverse (Figures 13 and 14). These are likely the best locations to observe and sample exposed impact melt outcrops formed by the Schrödinger impact event. Stops 6–9 are all located along the interior base of the uplifted peak ring of Schrödinger (Figures 13 and 14). These stops all provide an opportunity to examine and sample this peak ring material from boulder falls, several of which have distinct boulder trails indicating where the material originated (Figure 6). These stops would enable the rover to sample material from higher elevations in the peak ring that would be otherwise inaccessible. These stops are the best opportunity to gain insight into deep crustal lunar materials that were uplifted as the peak ring during basin formation. Finally, stops 10–12 all visit fresh impacts into the regolith on the basin floor, exposing both boulders and subsurface materials (Figure 14). Samples collected in each of the four sections of this proposed traverse would represent a diverse suite of materials that would fully address the main goals of the mission. From stop 12 the rover follows a direct return path to the lander owing to the relative proximity of the rover and lander at this point in the traverse and favorable terrain between the two. Upon return to the landing site the rover would deposit all collected samples into the return capsule to be sent back to Earth for additional laboratory-based analysis and sample preservation.

6.4. Optional Primary Mission Extended Traverse Paths

It is possible that by the time the rover were to reach stop 12 all systems would be functioning normally with ample mission time and sample space remaining. In this scenario, the proposed extended traverse path could be taken. The extended traverse path represents a much greater distance but allows the rover to access additional locations where material has been excavated by several small, well-preserved impact structures and ends the primary mission with a traverse path across nearly the entire width of the pyroclastic deposit. This extended traverse begins at stop 12 and heads south past two additional small impact craters in the basin floor (stops 13 and 14). At stop 15 the extended traverse path branches into three distinct options

shown as white, green, and orange dashed lines on the traverse map (Figure 13). It is unclear from available orbital data whether the rover will be able to safely traverse the hummocky terrain (deposit of Unit F) close to the peak ring (Unit A). Thus, stop 15 will serve as a navigational assessment point where in situ data collected by the rover, including high-resolution images and LIDAR scans of the terrain, will be used to determine the safest and most scientifically valuable path forward. Should high-resolution images reveal too many obstacles, or if the LIDAR scans show steep or uneven terrain, this optional traverse path would not be followed. Additionally, future remote sensing data sets could also be acquired before deployment of the proposed rover mission. These could include higher-resolution satellite images or terrain data collected by new orbital assets or even the descent stage of the proposed rover mission itself. The availability of higher-resolution data coverage for this region would give a better understanding of the hummocky terrain and determine whether this optional traverse path is viable before reaching the location with a rover.

The shortest of the three extended traverse path options is shown as a white dashed line on the traverse map (Figure 13). This path immediately turns west and heads back toward the pyroclastic vent. This portion of the path has been designed to enable multiple samples of pyroclastic material to be collected at varying distances from the main vent. These samples would enable compositional comparison and potentially identify the thickness of the pyroclastic layer across the entirety of the deposit. This extended traverse option is strategically positioned at the end of the primary mission traverse sequence, allowing any remaining sample space to be filled with pyroclastic regolith samples from this traversed cross section. In total, the extended traverse path including the white branch path is 41 km in length and would result in a total traverse distance of 85 km starting from and returning to the landing site. Again, assuming an average roving speed of 2 km hr^{-1} , this first extended traverse path dedicates 42.5 hr to driving time and splits the remaining 1087.5 hr evenly between all 31 SOIs along this route, for a maximum of 35 hr for science operations at each stop.

At stop 15, if a safe traverse route is available, the rover could instead follow the orange extended traverse path across the hummocky terrain of Unit F (Figure 13). This branch allows the rover to reach potential stops 3 and 4, visiting additional peak ring rock falls of varying composition. The orange path is 62 km in length, making for a total traverse distance of 106 km. This means that for the orange extended traverse path, a total of 53 hr would be dedicated to driving and the remaining 1077 hr of mission time could be split evenly between all 33 SOIs along this route, for a maximum of 33.5 hr at each stop.

If the hummocky terrain (Unit F) is determined to be too rough to traverse, but there is still ample time or sample space remaining, the rover could follow the third extended traverse option, represented by the green dashed line on the traverse map (Figure 13). This third extended traverse option from stop 15 would follow a path that continues south along the edge of the hummocky terrain to potential stop 2. This stop is situated among the most widespread boulder field in the region, which contains several of the largest boulders in the area. These boulders would be easily accessed by the rover and provide a plethora of potential sampling locations. After conducting analyses at potential stop 2, the rover would follow a similar

long traverse path across the pyroclastic deposits toward the main vent. This third option for an extended traverse path is 50.8 km in length, resulting in a total traverse distance of 94.8 km. Thus, for the green extended traverse path, a total of 47.4 hr would be dedicated to driving, while the remaining 1082.6 hr of mission time could be split evenly between all 31 SOIs along this route, for a total of 34.9 hr at each stop.

All optional traverse path branches reunite at stop 17. The final stops of the extended traverse path bring the rover close to the rim of the pyroclastic vent in order to obtain imagery of the vent interior. The walls of the vent itself are far too steep for the rover to maneuver down, so this suggested path stays a safe distance back from the rim. Stops 19 and 20 are included to serve both as locations for in situ observation of the pyroclastic vent and as navigational assessment points. Data collected here would be used to assess whether the rover is able to cross the large fissure to the north of the pyroclastic vent (Figure 14). After observing the vent interior, the rover would return to the initial landing site and transfer all collected samples to the ascent vehicle for return to Earth. Stops 19 and 20 are included with the expectation that during an extended mission phase the rover platform could continue on across the basin floor toward the mare deposits for additional surface analysis after completion of the primary mission.

6.5. Extended Mission Exploration Operations

The original HERACLES mission concept, on which this work was based, included a long-term goal of extending the mission timeline by sending multiple landers to different locations in Schrödinger within reach of the rover deployed with the first lander. This extended mission architecture would allow the rover to traverse to the landing side of a second lander and potentially deposit a second set of samples collected between the first and second landing sites. Regardless of the exact mission architecture implemented, the rover will be available to continue surface analyses following the safe transfer of the collected sample container to the ascent vehicle for return to Earth. From the final stop of the nominal or extended traverse paths at the landing site, the rover platform could retrace any previously taken path in order to revisit a previously observed site to collect additional observations using standoff instrumentation, or complete additional analyses of surrounding material. However, if there is no need for additional information collection within the previously visited area, we have included a potential extended mission path the rover could follow. This path is denoted by the dashed purple line in Figures 2 and 13. If deemed safe, the rover would cross the graben northwest of the landing site and continue northwest across the basin floor. This path includes several stops around a larger impact crater in the basin floor that may have excavated material from greater depths than the smaller craters visited along the nominal traverse (Figure 2). From this point, the extended mission traverse proceeds north toward the mare deposits (Unit C), where standoff measurements and analysis of the mare material could be conducted. Despite being of moderately high scientific importance, the deposits of mare material are not included in the nominal primary mission traverse plan, as they are located a significant distance from the other proposed sample locations. Analysis of the deposits of Unit C would answer questions directly related to science goals 2 and 3: lunar chronology and lunar volcanism. This extended mission traverse path totals 54.5 km in length from the landing

site to the mare and would likely take place over an additional two lunar days.

7. Conclusions and Summary

The morphologic mapping results presented here represent the most detailed and precise representation of morphologic units within the northern half of the Schrödinger peak ring produced to date. This map shows the extent and influence of volcanic units, including both pyroclastic and mare deposits, as well as the effect of post-Schrödinger impact cratering within this region. The small-scale inset map illustrates in great detail the different ejecta components of a small fresh impact crater located within the pyroclastic deposits.

This mapping effort has led to a better understanding of the distribution of materials within the central Schrödinger region. The knowledge of the extent, location, and diversity of surface features in this region has allowed for the creation of a sample rover traverse that accesses a diverse and scientifically significant suite of materials for analysis and sampling. The proposed threshold, nominal, and extended rover traverse paths, as well as the proposed landing zone, have all been carefully planned and mapped to provide precise locations for future rover operations. While the initial intent of this mapping and traverse planning effort was to support the HERACLES primary and extended mission plans, any future crewed or rover-based missions—including robotic precursor and post-precursor missions before and following a human mission—to Schrödinger basin could utilize this detailed mapping and the provided traverse plans as a basis for initial mission planning and eventual sample collection and return. This work adds to an extensive body of previous studies of the valuable geologic diversity present within Schrödinger and supports the inclusion of Schrödinger basin as a high-priority target for future lunar surface missions.

This work was carried out as part of contract No. 9F050-160981/001/TMB funded by the Canadian Space Agency. We would like to thank all the members of the PHASR maturation study team for their dedicated work and graduate students from the Institute for Earth and Space Exploration at Western University for their assistance in the site selection workshop. We extend special thanks to the LROC team for obtaining the images that enabled this work and the JMARS team for technical assistance and development of the GIS through which the maps presented here were produced. Finally, we thank the reviewers of this manuscript for their detailed and constructive comments throughout the review process.

ORCID iDs

Zachary R. Morse  <https://orcid.org/0000-0002-8713-580X>

References

- Allender, E. J., Orgel, C., Almeida, N. V., et al. 2019, *AdSpR*, **63**, 692
- Blewett, D. T., Lucey, P. G., Hawke, B. R., & Jolliff, B. L. 1997, *JGR*, **102**, 16319
- Boeder, P. A., & Soares, C. E. 2020, *Proc. SPIE*, **1148**, 1148903
- Chin, G., Brylow, S., Foote, M., et al. 2007, *SSRV*, **129**, 391
- Christensen, P. R., Engle, E., Anwar, S., et al. 2009, in AGU Fall Meeting (Washington, DC: AGU), IN22A-06
- Clegg, R. N., Jolliff, B. L., Robinson, M. S., Hapke, B. W., & Plescia, J. B. 2014, *Icar*, **227**, 176
- Ellery, A. 2016, Planetary Rovers (Berlin: Springer)

- Gaddis, L. R., Staid, M. I., Tyburczy, J. A., Hawke, B. R., & Petro, N. E. 2003, *Icar*, **161**, 262
- Head, J. W., & Wilson, L. 1992, *GeCoA*, **56**, 2155
- Head, J. W., Wilson, L., Deutsch, A. N., Rutherford, M. J., & Saal, A. E. 2020, *GeoRL*, **47**, e89509
- Hiesinger, H., Landgraf, M., Carey, W., et al. 2019, LPSC, **50**, 1327
- Hurwitz, D., & Kring, D. A. 2015, *E&PSL*, **427**, 31
- Kramer, G. Y., Kring, D. A., Nahm, A. L., & Pieters, C. M. 2013, *Icar*, **223**, 131
- Kring, D. A. 2013, EPSC, **8**, 714
- Kring, D. A., Kramer, G. Y., Bussey, D. B. J., & Hurley, D. M. 2014, LPICo, **1820**, 3057
- Kring, D. A., Kramer, G. Y., Collins, G. S., Potter, R. W., & Chandnani, M. 2016, *NatCo*, **7**, 13161
- Landgraf, M. 2016, HERACLES Mission Campaign Description, European Space Agency Official Document (Noordwijk: ESA)
- Lucey, P. G., Taylor, G. J., & Malaret, E. 1995, *Sci*, **268**, 1150
- McCubbin, F. M., Vander Kaaden, K. E., Tartese, R., et al. 2015, *AmMin*, **100**, 1668
- Melosh, H. J. 1989, Impact Cratering: A Geologic Process (New York: Oxford Univ. Press)
- Mest, S. C. 2011, *GSASP*, 477, 95
- National Research Council 2007, The Scientific Context for Exploration of the Moon (Washington, DC: National Academies Press)
- Needham, D. H., & Kring, D. A. 2017, *E&PSL*, **478**, 175
- O'Sullivan, K. M., Kohout, T., Thaisen, K. G., & Kring, D. A. 2011, *GSASP*, 477, 117
- Oberbeck, V. R. 1975, *RvGeo*, **13**, 337
- Osinski, G. R., Bourassa, M., Morse, Z. R., et al. 2019, in Proc. of the 70th Int. Astronautical Congress, 52715, <https://iafastro.directory/iac/browse/IAC-19/A3/2C/#paper.52715>
- Osinski, G. R., Grieve, R. A., Bleacher, J. E., et al. 2018, *JVGR*, **353**, 25
- Osinski, G. R., Tornabene, L. L., & Grieve, R. A. 2011, *E&PSL*, **310**, 167
- Potts, N. J., Gullikson, A. L., Curran, N. M., et al. 2015, *AdSpR*, **55**, 1241
- Prem, P., Hurley, D. M., Goldstein, D. B., & Varghese, P. L. 2020, *JGRA*, **125**, e06464
- Robinson, M. S., Brylow, S. M., Tschimmel, M., et al. 2010, *SSRv*, **150**, 81
- Rutherford, M. J., & Papale, P. 2009, *Geo*, **37**, 219
- Saal, A. E., Hauri, E. H., Cascio, M. L., et al. 2008, *Natur*, **454**, 192
- Schultz, P. H. 1976, *Moon*, **15**, 241
- Shankar, B., Osinski, G. R., Antonenko, I., & Neish, C. D. 2013, *CaJES*, **50**, 44
- Shoemaker, E. M., Robinson, M. S., & Eliason, E. M. 1994, *Sci*, **266**, 1851
- Steenstra, E. S., Martin, D. J., McDonald, F. E., et al. 2016, *AdSpR*, **58**, 1050
- Wetzel, D. T., Hauri, E. H., Saal, A. E., & Rutherford, M. J. 2015, *NatGe*, **8**, 755
- Wilhelms, D. E., Howard, K. A., & Wilshire, H. G. 1979, Geologic Map of the South Side of the Moon, USGS Investigations Map Series, **1162**
- Wilhelms, D. E., John, F., & Trask, N. J. 1987, *The Geologic History of the Moon, USGS Professional Paper*, 1348